

PNAS

www.pnas.org

Supplementary Information for

Human and climate influences on sediment transfers – a global account for the Holocene

Authors: Jean-Philippe Jenny, Sujan Koirala, Irene Gregory-Eaves, Pierre Francus, Christoph Niemann, Bernhard Ahrens, Victor Brovkin, Alexandre Baud, Antti E. K. Ojala, Alexandre Normandeau, Bernd Zolitschka, Nuno Carvalhais

Corresponding Author: Jean-Philippe.Jenny@inra.fr

This PDF file includes:

Supplementary text
Figures S1 to S9
Dataset S1 to S5
SI References

Supplementary Information Text

SAR as proxy of erosion

Sediment accumulation is the process of settling or being deposited to the basin floor, leading to the preservation of strata. Sediment particles originate from erosion and transport, or bio-precipitation (1). Long-term monitoring of sediment loads in rivers of the world provides a key source of evidence for assessing recent changes in soil erosion, but such records rarely extend back more than fifty years. Still, many opportunities exist to exploit the natural archives preserved within lake sediments, riverbanks, deltas, alluvial and colluvial soils to extend contemporary records, and provide evidence of changes in soil erosion over a range of time scales from decades to millennia. Among these archives, lake sediments can provide a consistent record of impact on erosion, given their normally continuous accumulation and their catchment-wide origins (2). An estimation of the quantity of material deposited in the lake may be difficult to interpret in terms of specific catchment-erosion relationships (3). Sediment reaching the lake bed will reflect not only the transport energy in the catchment but also the availability of sediment for erosion and the time lags in the system as material moves towards the lake bed via temporary sediment storage zones such as floodplains and deltas. SARs from lakes integrate three basic forms of sedimentary processes related to surface erosion, mass movement and linear transport. Assessment of the true catchment-derived sediment yield will require subtraction from the gross sediment yield of those components originating from lake margin erosion, the atmosphere and autochthonous production (3). These difficulties have led to several studies (e.g. 1) where sediment yields have been calculated by correlating synchronous levels in a large number of sediment cores to a master chronology; using density measurements to convert basin-wide estimates of sediment volume to sediment mass deposited over a specific time period from the catchment area (eg. $\text{t km}^{-2} \text{a}^{-1}$). The definition of past and present sedimentation areas in small lakes is likely to represent a large source of error in sediment yield calculations, especially where there is evidence that the sediment limit has changed because of water-level fluctuations. Hence, SAR data can only be used to infer, rather than to measure, rates and processes of erosion (2). Changes in vegetation and geomorphological transformation can alter the mode of transport from diffuse to microneckworks, or by creating gully erosion.

The Sadler effect may affect the interpretation of the SAR signal, but we assume that it has no strong effect on lake archives during the Holocene. The Sadler effect arises because of the incorporation of longer hiatuses in deposition (e.g. unsteady, discontinuous sedimentation) as averaging time is increased (5). However, continuous sedimentation generally characterize profundal lake sediment archives and when present, have often been noted in the original paper describing the record. The sediment supplies to a lake may be not continuous and, as time-scale increases, the time length of quiescence may also increase (which again would be consistent with the Sadler effect).

The Sadler effect is considered not affecting our results for several reasons. First, the Sadler theory is based on a compilation of SAR measurements taken in different locations for different time intervals and over much longer geological timescales, e.g. Ma, and for siliciclastic shelf deposits. On the other side, our results are based on variations of SAR within single lacustrine records. Second, mechanisms, such as lack of accommodation space, migration of deltas, tectonic, inferred by Sadler to explain the intermittent nature of deposition are less applicable to lakes, especially in the case of Holocene sedimentation for lakes with relatively small size of their watershed. Third, the Sadler effect is due to stochastic mechanisms, which is not compatible with the detection of synchronicity in the variation of SAR in our dataset. Fourth, the very existence of varved sequences in our dataset clearly show that intermittence of the sediment supply is not an issue. Five, the lengths of the records contributing to our dataset are more or less identical, i.e. 10 ka, which makes impossible that measured deposition rates decrease systemically with measurement duration. Six, hiatuses and events of instantaneous deposition were removed from the analysis when reported by the original authors.

Varved sites: proxy's sensitivity and high-resolution erosion trends

Our global synthesis (n = 632) of pollen representing 43,669 pollen samples, and 3,980 14C-dates has been implemented by a multi-proxy approach of annually resolved records at site level (n = 12, Fig. S8): Lake Belau (North Germany) (6), Lake Holzmaar (West Germany) (7), Lake Nautajärvi (southern Finland) (8), Lake of the Clouds (Minnesota, USA)(9), Lake Bosumtwi (Ghana, Africa) (10), Huguang Maar (South China) (11), Lake Xiaolongwan (Northeastern China) (12), Laguna Pumacocha (South America) (13), Lake Ahvenainen (South Finland) (14), Lake Van (East Turkey) (14), Elk Lake (Minnesota, USA) (15), and Black Sea (Eastern Europe) (16). In the case of Black Sea, sediment yields were first presented in Fig. S8 as it was in the original publication of Degens et al 1976, and then the data were normalized before statistical analyses.

Long records of SAR in lakes found in previously glaciated parts of Europe and North America tend to show high pre-Holocene SR declining to minimum values during the Early to Middle-Holocene (17). The arboreal pollen fractions show an increase from 12,000-10,000 cal. BP and 10,000 cal. BP to 8,000 cal. BP in Holzmaar and the Black Sea sites respectively, associated with a decrease of SAR. Erosion increased in Midwestern United States after European settlement (ca 1800-1850) (18). In Central and NW Europe, peaks in sediment flux often register Bronze Age, Iron Age, Medieval and Modern Times of farming, and these are comparable to the history of erosion deduced from studies of catchment geomorphology, archaeology and environmental history (17). This pattern is similar to the eastern seaboard of the USA, where pre-European settlements (pre-1740) saw sedimentation rates in estuaries that increased eight times through early deforestation and agriculture (1750–1820), and increase another three times during the period of peak deforestation and intensive agriculture (1820–1920) (19). For example, the Little Ice Age climate fluctuation is strongly implicated in driving increased flood activity in Lakes Atnsjøen, Norway (20). An early soil erosion signal was reported in two Middle Atlas lakes beginning about 4,000 cal. BP, possibly as pastoralism increased (21). In Eastern Europe, lake records the transition from natural to anthropogenic landscapes starting at the onset of the Greek 'Dark Ages' (~3,200 cal. BP) (22).

Varved sediments provide SAR data with annual resolution and seem well adapted to produce a very high-resolution signal to describe regional changes. Varved records were also used to perform a sensitivity analysis, and to show that SAR is a reliable proxy to assess the temporal variability of allochthonous supplies from the watersheds to the lakes. For those sites, SAR is explained by terrigenous supplies highlighted by Ti and Al concentrations, or magnetic susceptibility. Three Swedish lakes (not presented here) show that varve thickness is a good estimator of SAR and that SAR is not impacted strongly by changes in organic matter (23).

Temporal and spatial covariates

To estimate the contributions of environmental variables on SAR variations, several sources have been used. The spatial variables used as potential covariates are: 1) lake properties (i.e. watershed area, watershed:lake ratio, lake area, lake water residence time, discharge average, lake volume, shoreline development, average lake depth, elevation) (24); 2) erosion factors (i.e. C-factors, R-factors (rainfall erosivity factor) K-factors (soil erodibility factor)) (25) and LS-factors (topographic factors) were computed using the GRASS module in QGIS software (26) and the 10 km digital elevation model (DEM) provided in the HydroSHED database (24); 3) soil properties, i.e. total phosphorus, bulk density (fine earth), soil absolute depth to the bedrock, clay content, mass fraction, soil organic carbon content (fine earth), soil pH x 10 in KCL (27); and 4) climate variables, i.e. average temperature, precipitation, maximum temperature, max annual precipitation (28). The temporal variables used as potential covariates were described and referenced in the Numerical analysis section.

Supporting figures

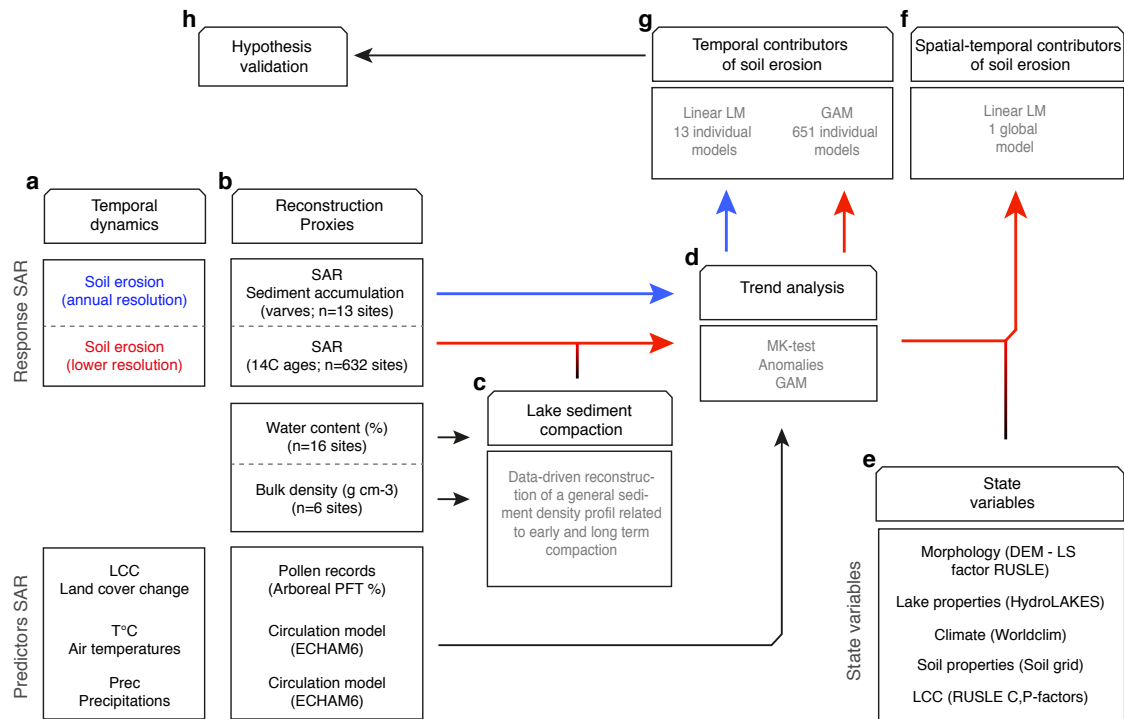


Fig. S1. Paleolimnological approach and strategy to identify contributors to sediment supply to lakes as proxy of erosion. (a) Trends reconstruction of soil erosion and of three hypothesized contributors of lake sedimentation and erosion dynamics (land cover, air temperature, and precipitation). (b) Reconstructed environmental variables: lake sediment accumulation rates (this study), water and density profiles, arboreal pollen (AP) percentage (this study), air temperatures and precipitation from MPI Earth System circulation model. (c) Parameters to correct lake sediment depths from compaction. (d) Reconstruction and analysis of the temporal dynamics of soil erosion and forcing factors (normalized data, per site respectively). (e) Spatial predictors of soil erosion. (f-g) Statistical investigation and quantification of the relationships between erosion and external drivers through GAM and validation of hypothesized contributors.

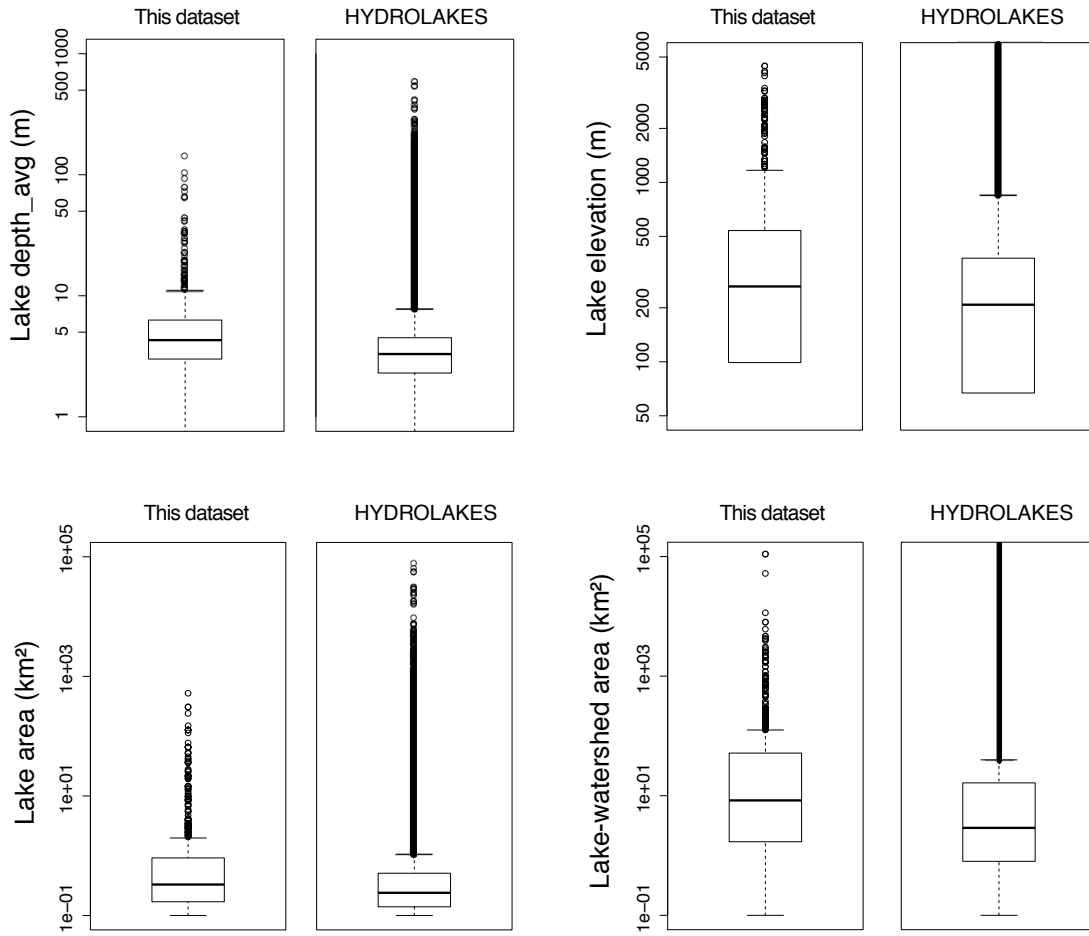


Fig. S2. Geomorphological and lake properties of our study sites from the pollen database (This dataset) compared to the 1.4 million lakes of the HydroLAKES database: lake depths, lake elevation, lake area, and watershed area. Our sample lake-catchment pairs captured a comparable range of morphometric properties relative to world lakes.

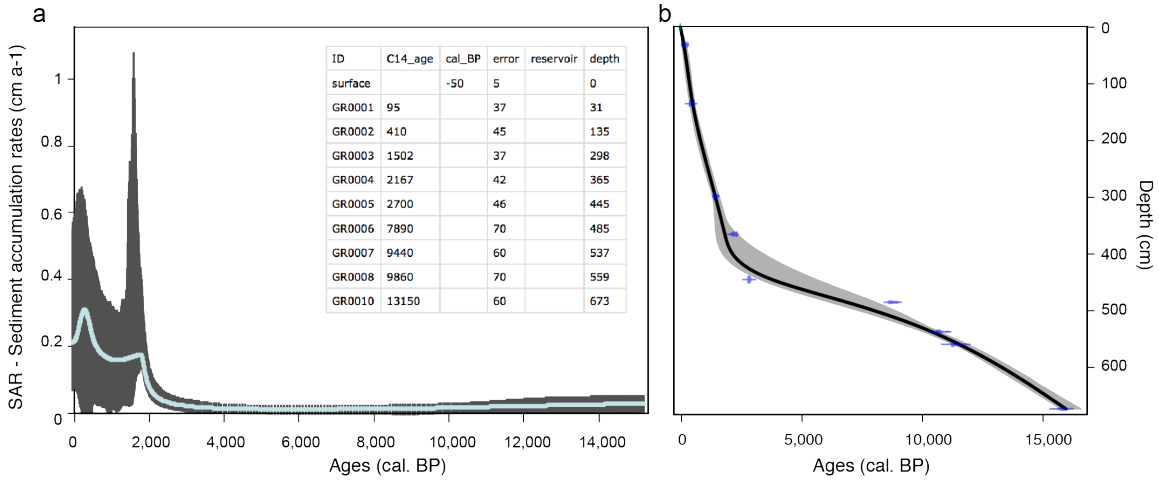


Fig. S3. Example for one site of SAR derived from 14C-dates. (a) SARs are plotted for the last 15,000 years. The SARs are derived from the 14C depth-age model (methods) (b), and the grey envelop shows the final 95% confidence intervals based on 1000 iterations. The dataset provides original data used to calculate the depth-age models: sample identifier (lab_ID), 14C dates (C14_date), related calibrated ages (cal_date), reported errors of radiocarbon dates (error), reservoir effect (reservoir) and sediment depth of the sample (depth).

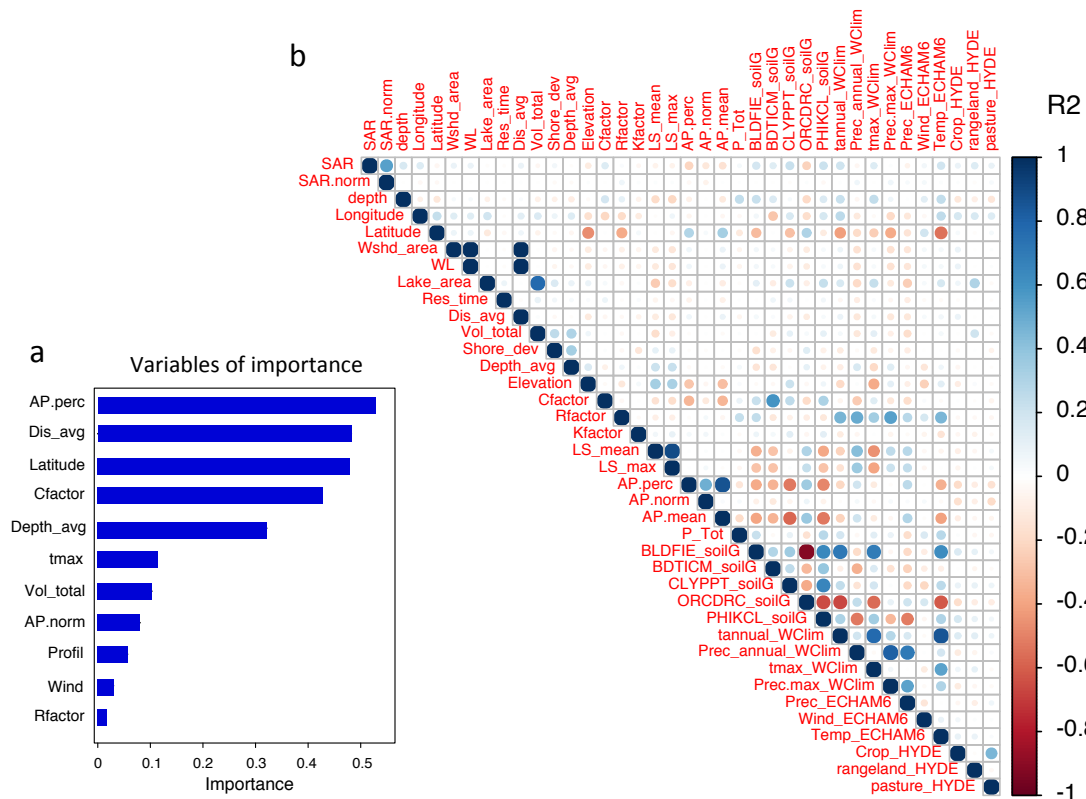


Fig. S4. Linear regression model and correlation matrix of SARs, temporal and spatial covariates. (a) Variables of importance (the absolute value of the t-statistic for each model parameter is used) show that SARs are explained best by land cover expressed as AP. SAR data (in cm a^{-1}) are not normalized. (b) The correlation matrix shows that AP are anticorrelated with SAR. Color scale documents the coefficient of determination. Large-sized circles correspond to lower p-values. Definitions of abbreviations are provided with Dataset S1.

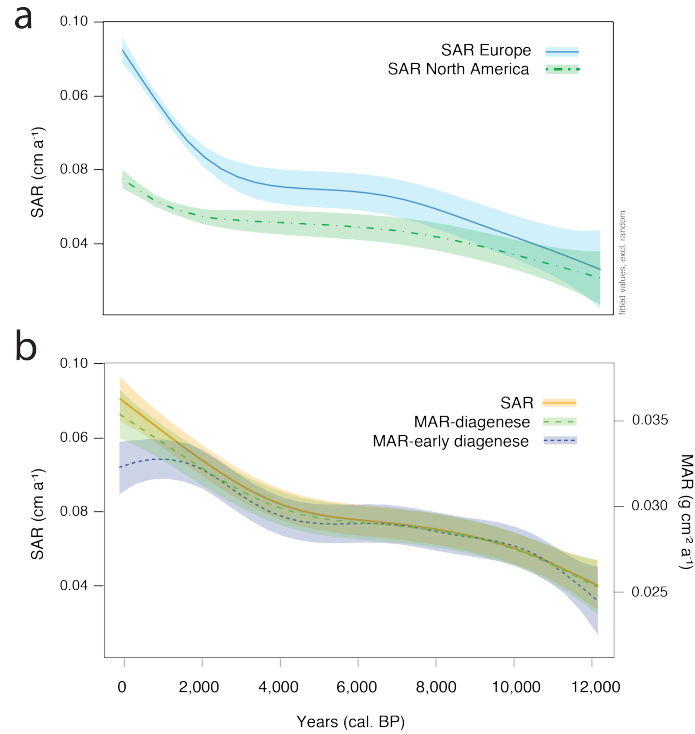


Fig. S5. Regional SAR trends for the Holocene. (a). Regional SAR trends reconstructed for Europe (blue line) and North America (use red color line) using GAM regressions. European sites show acceleration trends in SAR since 4,000 BP, whereas in North America erosion signals increased throughout the whole Holocene and accelerated at the end of the Holocene. Note that it was possible to reconstruct comprehensive regional trends despite a high heterogeneity among sites. (b) SAR trends, MAR trends, and MAR trends corrected for early compaction, using early compaction factor (compiled in this study, Fig. S8), and long-term compaction factor derived from Sadler (1981) (56).

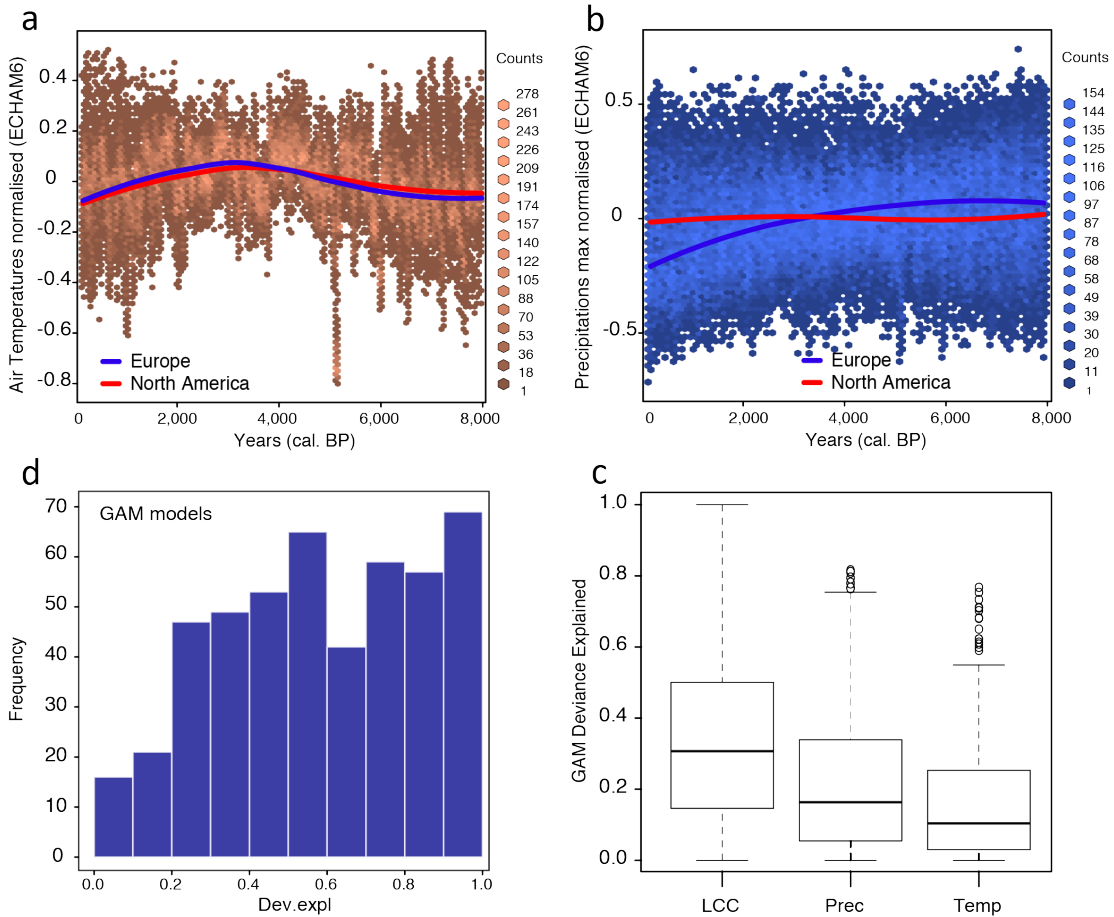


Fig. S6. Temporal trends for climate and land cover. Land cover and climate predictors of the SARs in our 632 sites. 8,000 years of mean annual air temperatures (a), maximum annual precipitation (b). (c) Deviance explained in the SAR trends by changes in land cover, precipitation and temperatures in the GAM models run for each of the 632 sites. All values correspond to site-specific anomalies and were used in the GAM analysis to disentangle impacts of climate and land cover drivers on erosion dynamics. (d) Histogram of deviances explained by the GAM models, run for each of the 632 sites.

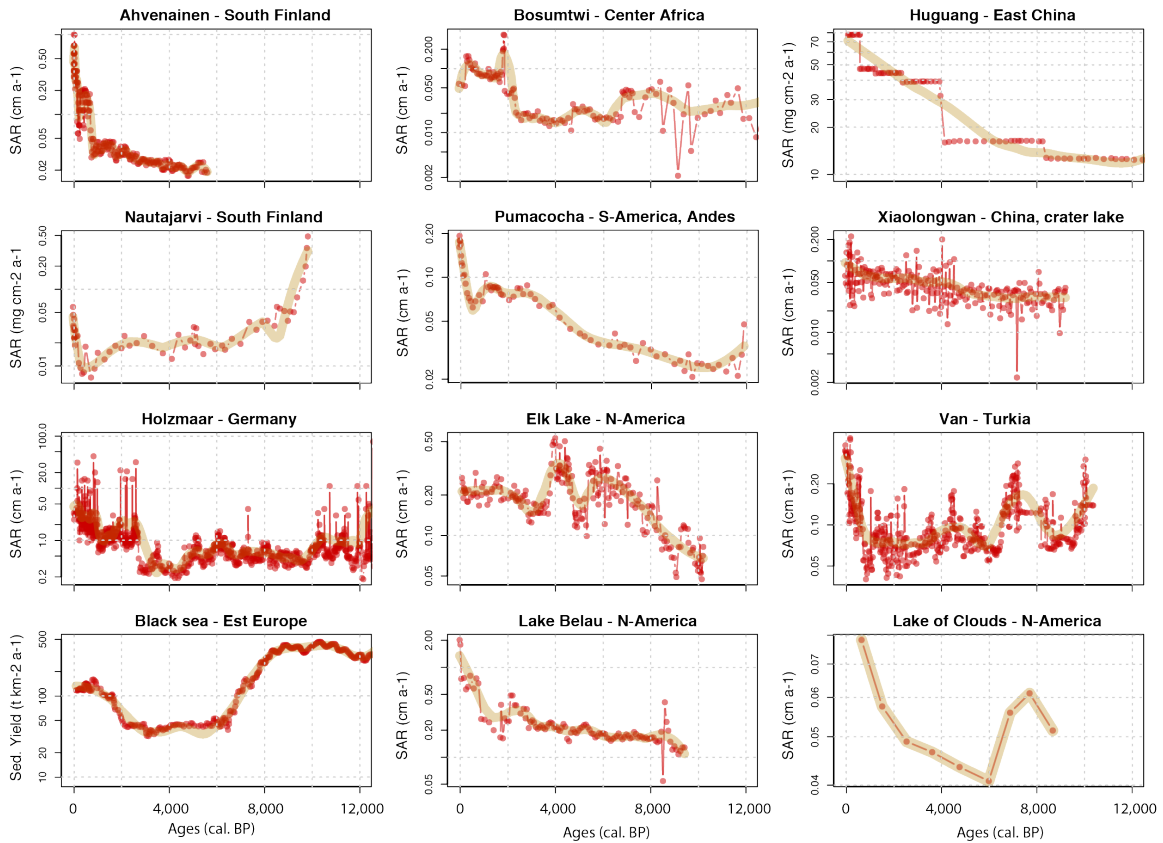


Fig. S7. Annual resolution trends in SARs based on varved sediment records: Lake Belau (North Germany)(35), Lake Holzmaar (Germany)(36), Lake Nautajärvi (southern Finland)(37), Lake of the Clouds (Minnesota, USA)(38), Lake Bosumtwi (Ghana)(39), Huguang Maar (South China)(40), Lake Xiaolongwan (Northeastern China)(41), Laguna Pumacocha (Peru, South America)(42), Lake Ahvenainen (South Finland)(43), Lake Van (East Turkey)(43), Elk Lake (Minnesota, USA)(44), and Black Sea (Eastern Europe)(45). When SAR data were not available, soil erosion was assessed based on sediment yields ($\text{t km}^{-2} \text{a}^{-1}$).

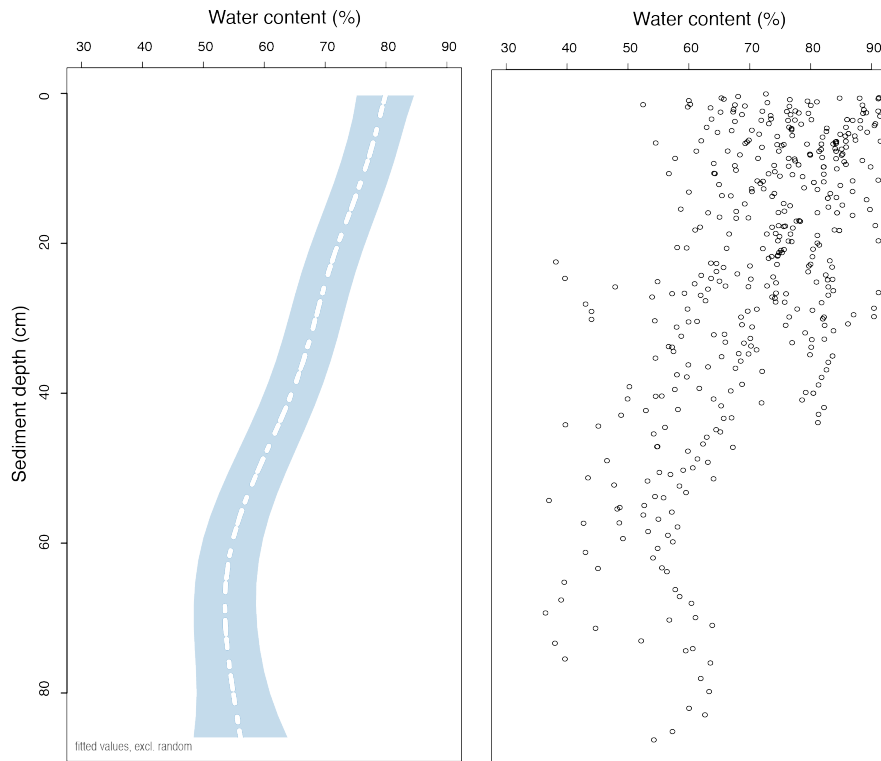


Fig. S8. Profiles of water content in 16 lake sediment cores, where data were available. The relation between water content and depth was used in this study to estimate the early sediment compaction effect on SAR trends (see method). Note that these data come from short sediment cores extracted by gravity corers. In our study, the compaction model is expected to over-estimate the compaction effect because SAR data were calculated for longer sediment cores and extracted most of the time by piston corers (see Dataset S2).

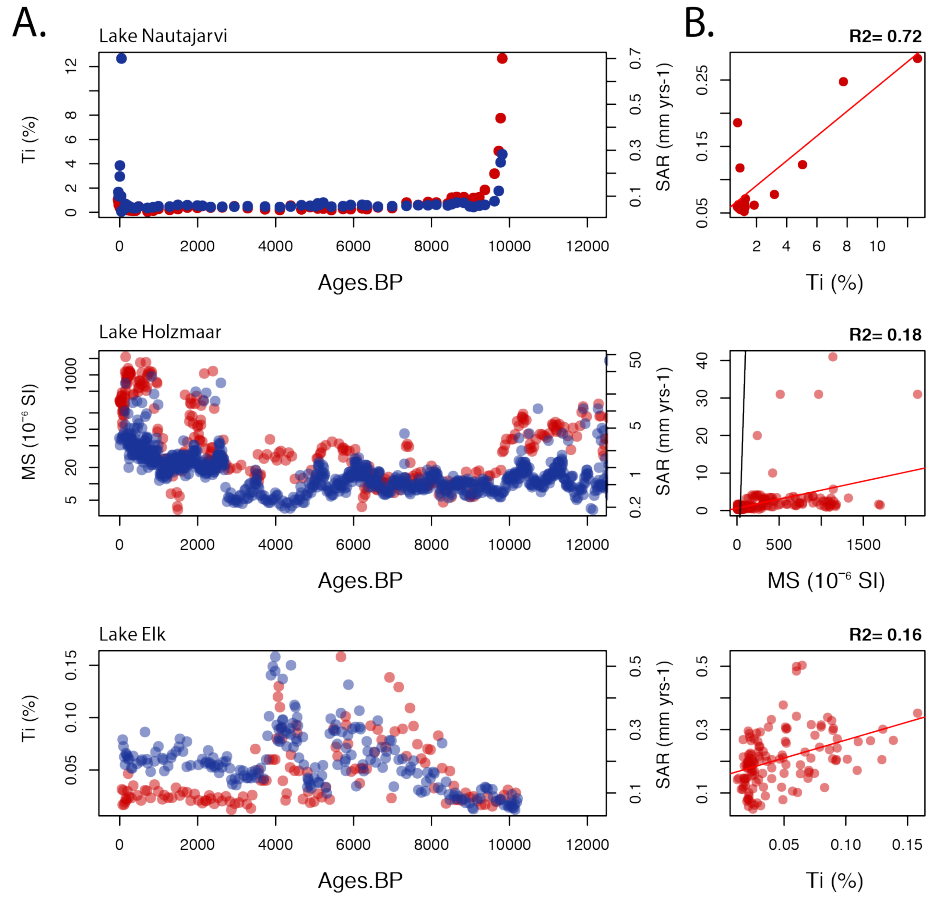


Fig. S9. Correlation between SAR and two independent proxies of allochthonous supplies to the lake: magnetic susceptibility (MS) and Titanium (Ti). A. Trends are provided for the Holocene. B. Pearson correlations between SAR and MS or Ti.

Supporting Datasets

Dataset S1. Description of input data. The variables are grouped in temporal and spatial variables. Variable names, units, resolution and source are provided, and data variables reconstructed or computed in this study are indicated. For temporal variables, the temporal resolution corresponds to the original resolution before resampling and harmonisation in 10 years intervals. The “high” error flag is a reminder that these reconstructions correspond to low frequency signals. In contrast, annual SAR reconstructions from varve records correspond to time series with high frequency signals, but are restricted to a small number of sites.

Dataset S2. Descriptive statistics of lake and catchment properties. 1st and 3rd quantile (1st Qu., 2nd Qu.), maximum (max.), mean, median, and minimum (min.) are represented for each of the properties. The number of data points before resampling of the full dataset (N across all sites) and per site (N per site*) are provided. Note that SARs were derived from depth-age models at 10 and 50 years resolution, which explain why the number of SAR estimates is greater than the 5,528 number of ages.

Dataset S3. Sites identification (ID) and description. These descriptions come directly from the three pollen databases. In addition, the new coordinates are reported because the original ones were generally few kilometers away from their respective lakes, as verified on satellite images (Note that for few lakes it was impossible to find the accurate location of the lake). The numbers of 14C-ages per profile are also reported.

Dataset S4. Sites spatial properties. The code and units for all variables are provided in Dataset S1.

Dataset S5. Original 14C ages and errors used to build the depth-age models. These original data are from the three pollen databases (see Dataset S1 for sources). The dataset provides original data used to calculate the depth-age models: original sample identifier (ID_original), 14C dates (C14_age), related calibrated ages (cal_BP), reported errors of radiocarbon dates (error), reservoir effect (reservoir) and sediment depth of the sample (depth), site identifier (E), chronology identifier (Chron), profil identifier (Profil), sample identifier for a given profile (Sample), sample thickness (Thickness), lake short name (Sigle), code of site type (Descriptor), sample date (SampDate), site name (SiteName).

Supporting references

1. McKee BA, Nittrouer CA, DeMaster DJ (1983) Concepts of sediment deposition and accumulation applied to the continental shelf near the mouth of the Yangtze River. *Geology* 11(11):631–633.
2. Edwards KJ, Whittington G (2001) Lake sediments, erosion and landscape change during the Holocene in Britain and Ireland. *CATENA* 42(2):143–173.
3. Dearing JA (1991) Lake sediment records of erosional processes. *Hydrobiologia* 214(1):99–106.
4. Bajard M, et al. (2017) Progressive and regressive soil evolution phases in the Anthropocene. *CATENA* 150:39–52.
5. Schumer R, Jerolmack DJ (2009) Real and apparent changes in sediment deposition rates through time. *J Geophys Res Earth Surf* 114(F3). doi:10.1029/2009JF001266.
6. Dörfler W, et al. (2012) A high-quality annually laminated sequence from Lake Belau, Northern Germany: Revised chronology and its implications for palynological and tephrochronological studies. *The Holocene* 22(12):1413–1426.
7. Zolitschka B (2003) Dating based on freshwater and marine laminated sediments. *Mackay Battarbee R Birks J Oldfield F Eds Glob Change Holocene Edw Arnold Publ Lond Pp* 92–106.
8. Ojala AEK, Alenius T, Seppä H, Giesecke T (2008) Integrated varve and pollen-based temperature reconstruction from Finland: evidence for Holocene seasonal temperature patterns at high latitudes. *The Holocene* 18(4):529–538.
9. Craig AJ Pollen Influx to Laminated Sediments: A Pollen Diagram from Northeastern Minnesota. *Ecology* 53(1):46–57.
10. Shanahan TM, et al. (2012) Late Quaternary sedimentological and climate changes at Lake Bosumtwi Ghana: New constraints from laminae analysis and radiocarbon age modeling. *Palaeogeogr Palaeoclimatol Palaeoecol* 361–362:49–60.
11. Mingram J, et al. (2004) The Huguang maar lake—a high-resolution record of palaeoenvironmental and palaeoclimatic changes over the last 78,000 years from South China. *Quat Int* 122(1):85–107.
12. Chu G, et al. (2014) Holocene cyclic climatic variations and the role of the Pacific Ocean as recorded in varved sediments from northeastern China. *Quat Sci Rev* 102:85–95.
13. Bird BW, Abbott MB, Rodbell DT, Vuille M (2011) Holocene tropical South American hydroclimate revealed from a decadal resolved lake sediment $\delta^{18}\text{O}$ record. *Earth Planet Sci Lett* 310(3):192–202.
14. O’Sullivan PE (1983) Annually-laminated lake sediments and the study of Quaternary environmental changes -- a review. *Quat Sci Rev* 1(4):245–313.
15. Dean WE (1999) The carbon cycle and biogeochemical dynamics in lake sediments. *J Paleolimnol* 21(4):375–393.
16. Degens ET, Paluska A, Eriksson E (1976) Rates of Soil Erosion. *Ecol Bull* (22):185–191.
17. Dearing JA, Jones RT (2003) Coupling temporal and spatial dimensions of global sediment flux through lake and marine sediment records. *Glob Planet Change* 39(1):147–168.
18. Heathcote AJ, Filstrup CT, Downing JA (2013) Watershed Sediment Losses to Lakes Accelerating Despite Agricultural Soil Conservation Efforts. *PLoS ONE* 8(1). doi:10.1371/journal.pone.0053554.

19. Syvitski JPM, Kettner A (2011) Sediment flux and the Anthropocene. *Philos Trans R Soc Lond Math Phys Eng Sci* 369(1938):957–975.
20. Nesje A, Matthews JA, Dahl SO, Berrisford MS, Andersson C (2001) Holocene glacier fluctuations of Flatebreen and winter-precipitation changes in the Jostedalbreen region, western Norway, based on glaciolacustrine sediment records. *The Holocene* 11(3):267–280.
21. Lamb HF, Damblon F, Maxted RW (1991) Human Impact on the Vegetation of the Middle Atlas, Morocco, During the Last 5000 Years. *J Biogeogr* 18(5):519–532.
22. Rothacker L, et al. (2018) Impact of climate change and human activity on soil landscapes over the past 12,300 years. *Sci Rep* 8(1):247.
23. Ojala AEK, Tiljander M (2003) Testing the fidelity of sediment chronology: comparison of varve and paleomagnetic results from Holocene lake sediments from central Finland. *Quat Sci Rev* 22(15):1787–1803.
24. Messenger ML, Lehner B, Grill G, Nedeva I, Schmitt O (2016) Estimating the volume and age of water stored in global lakes using a geo-statistical approach. *Nat Commun* 7:13603.
25. Naipal V, Reick C, Pongratz J, Van Oost K (2015) Improving the global applicability of the RUSLE model – adjustment of the topographical and rainfall erosivity factors. *Geosci Model Dev* 8(9):2893–2913.
26. GRASS Development Team, (2017) Geographic Resources Analysis Support System (GRASS) Software, Version 7.2. Open Source Geospatial Foundation. Electronic document.: <http://grass.osgeo.org>. Available at: <https://grass.osgeo.org/> [Accessed July 16, 2019].
27. Hengl T, et al. (2017) SoilGrids250m: Global gridded soil information based on machine learning. *PLOS ONE* 12(2):e0169748.
28. Fick SE, Hijmans RJ (2017) WorldClim 2: new 1-km spatial resolution climate surfaces for global land areas. *Int J Climatol* 37(12):4302–4315.